

Can oceanic reanalyses be used to assess recent anthropogenic changes and low-frequency internal variability of upper ocean temperature?

L. Corre · L. Terray · M. Balmaseda ·
A. Ribes · A. Weaver

Received: 20 August 2010 / Accepted: 23 November 2010 / Published online: 7 December 2010
© Springer-Verlag 2010

Abstract A multivariate analysis of the upper ocean thermal structure is used to examine the recent long-term changes and decadal variability in the upper ocean heat content as represented by model-based ocean reanalyses and a model-independent objective analysis. The three variables used are the mean temperature above the 14°C isotherm, its depth and a fixed depth mean temperature (250 m mean temperature). The mean temperature above the 14°C isotherm is a convenient, albeit simple, way to isolate thermodynamical changes by filtering out dynamical changes related to thermocline vertical displacements. The global upper ocean observations and reanalyses exhibit very similar warming trends (0.045°C per decade) over the period 1965–2005, superimposed with marked decadal variability in the 1970s and 1980s. The spatial patterns of the regression between indices (representative of anthropogenic changes and known modes of internal decadal variability), and the three variables associated with the ocean heat content are used as fingerprint to separate out the different contributions. The choice of variables provides information about the local heat absorption, vertical distribution and horizontal redistribution of heat, this latter being suggestive of changes in ocean circulation. The discrepancy between the objective analysis and the reanalyses, as well as the spread among the different

reanalyses, are used as a simple estimate of ocean state uncertainties. Two robust findings result from this analysis: (1) the signature of anthropogenic changes is qualitatively different from those of the internal decadal variability associated to the Pacific Interdecadal Oscillation and the Atlantic Meridional Oscillation, and (2) the anthropogenic changes in ocean heat content do not only consist of local heat absorption, but are likely related with changes in the ocean circulation, with a clear shallowing of the tropical thermocline in the Pacific and Indian oceans.

Keywords Anthropogenic climate change · Internal variability · Oceanic reanalyses · Observations · Upper ocean temperature

1 Introduction

Identifying and quantifying the impact of anthropogenic forcing on the global ocean have become of critical importance. A large fraction of the energy gained by the Earth climate system during the twentieth century has accumulated in the world subsurface oceans (Bindoff et al. 2007). In order to achieve a rigorous estimation of the Earth's energy balance, monitoring the variations of ocean heat content at both global and regional scales is essential. The future rate of ocean heat uptake is also of primary importance as it dictates the lagged response of surface temperature rise. Recent observational studies show that some of the expected modifications due to anthropogenic forcing may already have been emerging over the last few decades. The most prominent signal is the increase in global ocean heat content as a result of anthropogenic forcing (Barnett et al. 2005; Levitus et al. 2005). A number of observational estimates show a gradual warming of the

L. Corre (✉) · L. Terray · A. Weaver
Cerfacs-CNRS, 42 Av. G. Coriolis, 31057 Toulouse, France
e-mail: lola.corre@cerfacs.fr

M. Balmaseda
E.C.M.W.F, Shinfield Park, Reading RG2 9AX, UK

A. Ribes
CNRM-GAME, Météo France-CNRS,
42 Av. G. Coriolis, 31057 Toulouse, France

upper ocean (0–700m) heat content superimposed with decadal variations (Ishii et al. 2003; Levitus et al. 2005; Bindoff et al. 2007). Beyond the general analyses consistency, accounting for their differences is of great interest in order to shed light on uncertainties in the recent ocean evolution. Differences may come from many factors such as the choice of input data, quality control, infilling method, and/or instrumental bias correction (Palmer et al. 2010). The latter have been produced to minimize instrument-related biases due to changing technologies used to collect ocean temperature profiles. The most well-known instrument bias is the significant, time varying, warm bias in the abundant but low accuracy temperatures collected by expendable bathythermograph (XBT) (Gouretski and Koltermann 2007). This bias is responsible for some of the observed temperature fluctuations in the 1970s. Different methods for correcting XBTs have been proposed, based on correcting fall-rates (Wijffels et al. 2008; Ishii and Kimoto 2009), or reported temperatures (Levitus et al. 2009). Most corrections result in a reduction of the global ocean heat content interdecadal variability. However, effect on the long-term trend estimates vary from one correction type to another. According to Levitus et al. (2009), their corrections have little effect on the trend estimate. On the contrary, Domingues et al. (2008) find an ocean warming rate, from 1961 to 2003, about 50% larger than equivalent rate of non-corrected estimates when using Wijffels et al. (2008) corrections. By comparing the ocean heat content from different observed datasets, Lyman et al. (2010) estimated uncertainties arising from the choice of climatology, the choice of mapping methodology, the effects of irregular and sparse sampling, the method of XBT correction and XBT quality control. They find that uncertainties in XBT bias corrections are the dominant error source over the period 1993–2008.

Most of the studies cited above are objective analyses based solely on observations and use statistical methods to fill the data sparse regions. Yet, statistical infilling introduces uncertainties as different infilling methods lead to different results (AchutaRao et al. 2007). Oceanic reanalyses are an alternative to purely statistical approaches which are used to reconstruct the 4-dimensional structure of the global ocean. Constructing an oceanic reanalysis consists of simulating the evolving ocean state with an ocean model driven by the best available atmospheric surface forcing and constrained by assimilating direct observations. In that case, the infilling of the data sparse regions is also based on the physics of ocean models. Ocean reanalyses thus provide a time-continuous, dynamically-interpolated estimate of the ocean state and include the influence of the evolving atmospheric state on subsurface ocean variables. This physically-based approach has proved worthwhile in providing spatially complete fields. Carton and Santorelli

(2008) examined the evolution of the temperature in the upper 700 m of the global ocean as represented by two objective analyses and seven model-based oceanic reanalyses. They discussed the relative role of natural variability, analysis method and data inadequacies in the main uncertainties associated with the recent upper ocean warming. Within the European ENACT and ENSEMBLES projects, global multi-decadal ocean reanalyses have been produced to provide initial conditions for coupled model forecasts on seasonal to decadal time scales (Davey et al. 2006). This set of reanalyses provides a probabilistic estimate of the changing ocean state over the past decades. A first set of ENACT reanalyses has been compared in terms of globally averaged temperature over the top 300 m from 1960 to 2000 (Davey et al. 2006). Results highlight the substantial progress that has been made in reconstructing recent changes in upper ocean heat content. In most regions, differences between reanalyses are substantially less than the amplitude of interannual variability. Nevertheless, understanding similarities and differences between reanalyses is needed to improve each product and increase the value of ocean state estimates. This is a difficult task as many factors can be involved such as model errors, problems associated with the assimilation systems and/or with the atmospheric forcings, biases and scarcity of the observations.

This paper further examines recent upper ocean changes using five model-based ocean reanalyses and a model-independent objective analysis. We use the mean temperature above the 14°C isotherm (Tiso14 thereafter) as a measure of the recent ocean warming. Based on the analysis of the EN2 observational dataset (Ingleby and Huddleston 2007) between 1965 and 2005, Palmer et al. (2007) show an average warming trend of 0.043°C per decade for this variable. As Tiso14 is independent of the absolute reported depth, the analysis of this variable in products derived only by the observations is insensitive to the XBT's fall-rate errors. Moreover, compared with more classical fixed depth mean temperatures, Tiso14 has been proved valuable to isolate externally forced air–sea heat fluxes changes by filtering temperature modifications induced by dynamical processes (Palmer and Haines 2009). By reducing the influence of ocean circulation changes, Tiso14 also improves observation-model comparison and allows a robust detection of both natural and anthropogenic influences on ocean subsurface temperatures changes (Palmer et al. 2009). The detection of climatic changes is based on the ability of separating the influence of each of the different climatic forcings. Different approaches have been proposed to isolate the low frequency signal associated with anthropogenic forcing. The first commonly used is to represent it by a linear trend (Enfield et al. 2001; Sutton and Hodson 2005; Knight et al. 2006). This approach assumes that the anthropogenically forced signal

is uniform and linear over time, thereby including the non-linear part of the trend in the noise. A second method consists of characterizing the anthropogenically forced signal by a simple index, using for example the global mean sea surface temperature (Trenberth and Shea 2006; Mann and Emanuel 2006). In order to account for the spatial non uniformity of the anthropogenically forced signal, Ting et al. (2009) regress the two dimensional fields they want to analyze on the time series of globally averaged SST. Here we will follow a similar approach, but construct an anthropogenically forced signal index with the Tiso14 variable from climate model scenarios [based on Ribes et al. (2009) method]. This method as well as the observed and reanalysis data used are briefly described in the next section. The time evolving upper ocean temperature is simply investigated in terms of linear trend and decadal variability in Sect. 3. Section 4 focuses on the spatial pattern of the changes, isolating both the anthropogenically forced signal and internal variability. Section 5 is a summary of our main results.

2 Data and method

2.1 Observations

The first analysis (hereafter referred to as EN3-OA) is a statistical objective analysis, independent of a numerical model, based on the version EN3_v2a of the ENACT/ENSEMBLES quality-controlled dataset which is an updated version of the EN2 dataset described by Ingleby and Huddleston (2007). Most data are from the World Ocean Database 2005, completed by profiles from the Global Temperature-Salinity Profile Program and the US-GODAE Argo Global Data Assembly Center. The final dataset is composed of mechanical bathythermographs (MBTs), expendable bathythermographs (XBTs), hydrographic profiles (CTDs and predecessors), moored buoys from the TAO/TRITON and PIRATA arrays and profiling floats including Argo data since 2000. Instrument-dependent corrections are applied using an automated quality control system. In particular, corrections are applied to XBT profiles based on the corrected fall-rate equation proposed by Hanawa et al. (1995) and additional bias corrections (Thadathil et al. 2002; Kizu et al. 2005). The spatial coverage of the EN3_v2a dataset temperature profiles, from 1960 to 2005, is illustrated in Fig. 1. During the first 5-year periods, the coverage is very poor, with large data sparse regions such as the South Hemisphere and the Tropics. In contrast, the North Atlantic is well observed, especially along ship tracks. Progressively, the data coverage increases over time. We can see the apparition of the TAO arrays in the Tropical Pacific between 1985 and 1989.

At the end of the period, the development of Argo floats provides an almost global coverage, with the exception of the polar regions and marginal seas. Note also that the coverage is better in the Northern Hemisphere than in the Southern Hemisphere.

2.2 Reanalyses

Temperature fields from the EN3-OA observational product are compared with three ENSEMBLES reanalyses (CERFACS, ECMWF and INGV) and the SODA reanalysis. The ENSEMBLES reanalyses are based on the assimilation of in-situ temperature and salinity profiles from EN3_v2a dataset. Atmospheric forcings fields consist of daily fluxes of momentum, heat and fresh water derived from the ERA-40 reanalysis (Uppala et al. 2005). Additional bias correction terms are applied to precipitation (Troccoli and Källberg 2004). From September 2002 onwards, when ERA40 terminates, ECMWF operational surface fluxes are used. The sea surface temperature is strongly restored to analyzed SST maps derived from the OIv2 SST product (Reynolds et al. 2002). A globally uniform relaxation coefficient of $-200 \text{ W m}^{-2} \text{ K}^{-1}$ is used, which corresponds to a relaxation time-scale of 12 days for a mixed-layer depth of 50 m. A common initialization sequence ('spinup') is also prescribed, starting on 1 January 1953. It uses ERA40 climatological surface fluxes up to 1 January 1958, and then the daily ERA40 surface fluxes from 1 January 1958 to 31 December 1961 (Davey et al. 2006). During spinup, relaxation terms to prescribed temperature and salinity fields are imposed, as described further for each reanalysis.

The ENSEMBLES reanalyses differ from each other since they are produced by different data assimilation systems and ocean general circulation models (summarized in Table 1). Other differences may also come from different formulations in subsurface relaxation to climatology. CERFACS and INGV employed the Ocean Parallelise (OPA) version 8.2 ocean model (Madec et al. 1998). CERFACS uses the OPAVAR assimilation system (Daget et al. 2009), a multivariate three-dimensional (3D) variational data assimilation system. INGV uses the INGV-CMCC Global Ocean Data Assimilation System which consists of a multivariate reduced order optimal interpolation scheme (Bellucci et al. 2007) where the order reduction is based on the state vector projection onto vertical empirical orthogonal functions (De Mey and Benkiran 2002). For both CERFACS and INGV, a weak global subsurface relaxation to gridded temperature and salinity monthly climatology (Levitus et al. 2005) is applied with a 3-year timescale. ECMWF is based on a 3D optimal interpolation scheme (Balmaseda et al. 2008b) combined with the Hamburg Ocean Primitive Equation (HOPE)

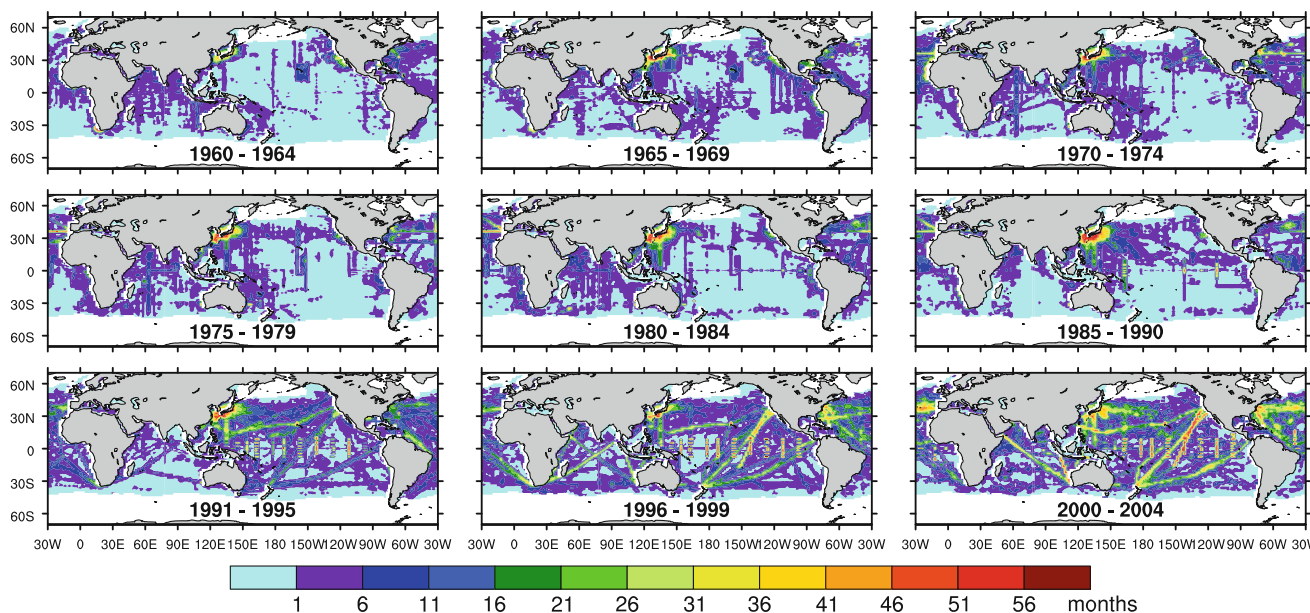


Fig. 1 Number of months per pentad for which at least one temperature profile from EN3_v2a dataset gives a value for Tiso14

ocean model (Wolff et al. 1997). A special feature of the ECMWF reanalysis is the assimilation of altimeter data from 1993 onwards (Le Traon et al. 1998). The subsurface relaxation to climatology is applied with a 10-year time-scale. This weak relaxation is possible because a prescribed a priori bias correction to temperature, salinity and pressure-gradient is added. In order to sample uncertainties in estimates of the observed state of the ocean, each individual reanalysis does not consist of a single simulation but of several ensemble members. Ensemble members are created by using multiple atmospheric fields whose differences were constructed to be consistent with estimates of the uncertainty in these fields (Daget et al. 2009). Sets of perturbations for sea surface temperature, wind stress, and freshwater flux were produced. The CERFACS reanalysis uses the three sets of perturbations and consists of a nine-member ensemble. ECMWF and INGV only uses wind stress perturbations and contains five and three ensemble members, respectively. Examination of the global upper averaged temperature of the ENSEMBLES reanalyses show a clustering of ensemble members issued from a same system (Murphy et al. 2009). This result indicates that the application of the perturbation strategy to any single reanalysis system is probably not sufficient to sample fully the true uncertainty in the observed ocean state. In this regard, the spread among individual ENSEMBLES reanalyses may provide a more realistic estimate of the uncertainty. Hereafter, we will only consider the non-perturbed member of each ensemble.

The Simple Ocean Data Assimilation (SODA) product, version 2.0.2-4 (Carton and Giese 2008) uses a model

based on the Parallel Ocean Program numerics (Smith et al. 1992) whose resolution is eddy-permitting. It is driven by ERA-40 winds and surface freshwater flux from the Global Precipitation Climatology Project monthly satellite-gauge merged product (Adler et al. 2003). A relaxation to the World Ocean Atlas 2001 (Boyer et al. 2002) climatological sea surface salinity is applied with a 3-month relaxation time scale. The mixed layer temperature is updated with near-surface temperature observations. The assimilated dataset consists of approximately 7×10^6 temperature and salinity profiles. Two-thirds of the data are from the World Ocean Database 2001 (Boyer et al. 2002; Stephens et al. 2002), completed by real-time temperature profile observations from the National Oceanographic Data Center (NODC)/NOAA temperature archive. The correction to the XBT's fall-rate equation provided by Hanawa et al. (1995) is included.

As mentioned in the Introduction, observational datasets are affected by instrumental biases. With the aim of reducing those biases, a new version of the EN3_v2a dataset has been produced (<http://hadobs.metoffice.com/en3/>). It has removed the cold water tapering (Thadathil et al. 2002) that is applied to some XBT corrections. Then, the corrections to XBT depths from Table 1 of Wijffels et al. (2008) have been applied. This corrected dataset has been used in a new reanalysis hereafter referred to as ECMWF_update. Model, data assimilation technique, atmospheric forcing and restoring coefficients are similar to those described for the ECMWF reanalysis. Comparison between the two products gives an estimate of the impact of the XBT warm bias on upper ocean heat content decadal variability and trends.

Table 1 Reanalyses considered in this study

Reanalysis	Model, resolution	Surface fluxes	Data	Assimilation system
SODA v. 2.0.2-4	POP 2.1 0.25° × 0.4° 40 levels	ERA-40 winds GPCP freshwater flux	WOD01 NODC/NOAA archive	Sequential
CERFACS	OPA v. 8.2 ORCA 2°: 2° × 2°–0.5° 31 levels	ERA-40 daily flux corrected precipitations after 2001: ECMWF fluxes	ENACT/ENSEMBLE dataset v. EN3_v2a	OPAVAR 3-dimensional variational
INGV	OPA v. 8.2 ORCA 2°: 2° × 2°–0.5° 31 levels	ERA-40 daily flux corrected precipitations after 2001: ECMWF fluxes	ENACT/ENSEMBLE dataset v. EN3_v2a	Reduced order optimal interpolation
ECMWF	HOPE 1° × 1°–0.3° 29 levels	ERA-40 daily flux corrected precipitations after 2001: ECMWF fluxes	ENACT/ENSEMBLE dataset v.EN3_v2a altimeter data	3D optimal interpolation
ECMWF_update	HOPE 1° × 1°–0.3° 29 levels	ERA-40 daily flux corrected precipitations after 2001: ECMWF fluxes	ENACT/ENSEMBLE dataset v.EN3_v2a XBT corrections (Wijffels et al. 2008) altimeter data	3D optimal interpolation

Thereafter, the temperature and isotherm depth fields used correspond to monthly means after interpolation to a common grid of resolution 1° longitude, 1° latitude, 33 levels

2.3 Statistical method

Observational coverage prior to the introduction of XBTs in the late 1960s was particularly poor (Fig. 1), so we exclude the period 1960–1965 in all our statistical calculations. Moreover, since the focus of this study is on low frequency variability and change, all fields are low-pass filtered with a 5-year cutoff frequency. Those methodological choices are the same as in Palmer et al. (2007), whose results are thus quantitatively comparable with ours (Sect. 3). For the three variables analyzed, which are Tiso14, the depth of the 14°C isotherm (Diso14) and the 250 m mean temperature (T250m), only areas where the 14°C isotherm is different from zero depth for the whole period are used for calculations. In Sect. 4 we attempt to assess the causes of the recent upper ocean temperature change, and to describe the associated spatial patterns. In particular, we aim to estimate the upper ocean response to an anthropogenically forced signal. The first step is to base the analysis on Tiso14 which filters out dynamical processes and so isolates the externally forced air-sea heat flux changes. The second step consists of regressing the Tiso14 field on the best possible index characterizing the temporal response of the climate system to anthropogenic forcing. This index, hereafter denoted by μ , is evaluated from the global 5-year low-pass filtered monthly mean Tiso14 of Atmosphere-Ocean general circulation models (AOGCMs) simulations and scenarios included in the WCRP CMIP3 (Coupled Models Intercomparison Project) multimodel

archive of the Program for Climate Model Diagnosis and Intercomparison (<http://www.pcmdi.llnl.gov/>), that cover the 1901–2009 period. From 1901 to 1999, we use the AOGCMs twentieth-century simulations. Over this period, the CMIP3 simulations differ by the external forcings they take into account. We exclude AOGCMs that take into account natural forcings (mainly changes in solar irradiance and changes due to explosive volcanic eruptions). As a result, the nine selected AOGCMs (see Table 2) only take into account anthropogenic forcings over the twentieth century. For the 2000–2009 period, we use the A1B scenario from the same nine AOGCMs. The A1B scenario only prescribes some anthropogenic forcings, that are identical for all models.

By computing μ from the Tiso14 variable, we take advantage of the ocean's integrative capacity, which produces high signal-to-noise ratios (Banks and Wood 2002). To filter out a large part of the internal variability, μ is assumed to be smooth. Such an assumption can be justified by the fact that the largest part of the anthropogenic forcing is due to greenhouse gases emissions, which have been increasing gradually over the twentieth century. The estimate of this smooth pattern is based on smoothing splines with four equivalent degrees of freedom; all details about the method and underlying assumptions can be found in Ribes et al. (2009). Denoting by s and t the spatial and temporal indices, we assume the following decomposition of the observed climate (denoted by ψ):

Table 2 AOGCMs used together with their originating group

IPCC I.D.	Center and location
bccr_bcm2_0	Bjerknes Centre for Climate Research (Norway)
ccma_cgcm3_1	Canadian Centre for Climate Modelling and Analysis (Canada)
ccma_cgcm3_1_t63	Canadian Centre for Climate Modelling and Analysis (Canada)
cnrm_cm3	Météo-France, Centre National de Recherches Météorologiques (France)
csiro_mk3_5	CSIRO Atmospheric Research (Australia)
giss_aom	NASA/Goddard Institute for Space Studies (USA)
ingv_echam4	Instituto Nazionale di Geofisica e Vulcanologia (Italy)
ipsl_cm4	Institut Pierre Simon Laplace (France)
ukmo_hadcm3	Hadley Centre for Climate Prediction and Research (USA)

$$\psi(s, t) = g(s) \cdot \mu(t) + \epsilon(s, t),$$

where g can be considered as the spatial pattern of the anthropogenically forced climate change and ϵ represents the natural variability. The latter could be decomposed between the response to natural external forcings (mainly solar irradiance and volcanic eruptions) and natural internal variability. Here, we assume that the internal variability is dominating as the combined effect of natural forcings explain only a small fraction of the observationally based estimates of the increase in ocean heat content (Hegerl et al. 2007). The above equation relies upon a time-space separability assumption (Ribes et al. 2009) of the climate response to anthropogenic forcing. From g , estimated by regression of ψ on μ , we can estimate the spatial pattern and amplitude (δ) of the anthropogenically forced climate change, between January 1965 (denoted by ti) and December 2005 (denoted by tf):

$$\delta(s) = g(s) \cdot (\mu(tf) - \mu(ti)).$$

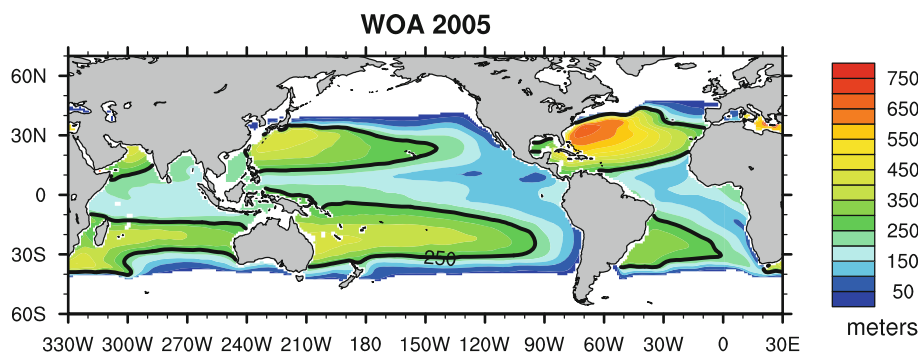
3 Global and basin-averaged upper-ocean temperature changes

We first look at the evolution of the mean temperature of all the water warmer than 14°C. Figure 2, which shows Diso14 in the world ocean, helps to illustrate the volume of water considered. High latitudes are naturally excluded by the study as sea water temperature never reaches 14°C there. Elsewhere, the average Diso14 is around 250 m, with large regional contrasts. Maximum depths are found to the west of the subtropical gyres, reaching more than 600 m in the North Atlantic, whereas it is above 150 m in equatorial and coastal upwelling regions: around the

equator and on the east side of the Pacific and the Atlantic basins.

The evolution of Tiso14 over the period 1960–2005, as seen by the three ENSEMBLES reanalyses and SODA, is shown Fig. 3. In general, the ensemble spread is small compared with the signal. In the Atlantic ocean there is a sharp increase in spread toward the end of the period. It derives primarily from ECMWF which exhibits cooler anomalies than the others from 1993 onwards. This specific behavior is consistent with the impact of altimeter, as indicated by observing system experiments (OSEs) conducted with the ECMWF system. The effect of altimeter data assimilation will be discussed in more details later in the text in relation with Fig. 4. Except for this feature of the ECMWF system, the ENSEMBLES reanalyses share the same atmospheric forcings and assimilated observations. Their spread gives a rough estimate of uncertainties associated with data assimilation systems (including the ocean model and data assimilation methods). As they are based on the same ocean model (they only differ by their assimilation schemes) CERFACS and INGV results are close to each other. Observations assimilated in SODA are different from the ones used in the ENSEMBLES reanalyses. Thus, the comparison with SODA reflects in a qualitative way uncertainties associated with observations. It increases uncertainty estimates before 1970, where the SODA time series is below the ENSEMBLES spread. SODA also exhibits the most pronounced maximum warming around 1980 and 1990. This may be linked to the additional XBT correction terms (Thadathil et al. 2002; Kizu et al. 2005) applied to the EN3_v2a profiles and which are not used in SODA. Despite these discrepancies, the various Tiso14 time series show a high degree of consistency with each other. This general similarity allows us to define a MEAN reanalysis, calculated as the average of those four individual model-based reanalyses. At the global scale, the MEAN reanalysis exhibits a Tiso14 warming trend of 0.045°C per decade superimposed on decadal variations of 0.028°C amplitude (Table 3). Note that the amplitude of the decadal variability is computed as the standard deviation of the detrended 5-year low-pass filtered time-series. Results are very similar for the model-independent objective analysis with a global trend of 0.046°C per decade and decadal variability of 0.030°C standard deviation. In all the basins, the MEAN and EN3-OA Tiso14 curves are very highly correlated. In the well-sampled basins (the Atlantic basin over the whole period and the Pacific basin after 1980), the two curves are almost similar. This is also true for T250m and Diso14 (not shown). Indeed, for both variables, correlations between the MEAN and EN3-OA curves are around 0.9 in all the basins.

Fig. 2 Mean depth (m) of the 14°C isotherm during 1960–2005, computed from the World Ocean Atlas 2005 (WOA05) climatology. The black line indicates locations where the 14°C isotherm equals 250 m



3.1 Decadal variability

The origin of decadal variability of the global ocean temperatures has long been debated. Here we use the comparison of Tiso14 with T250m, Diso14, and the sea surface temperature (SST) from the HadSST2 data set (Rayner et al. 2006) (Fig. 4) to discuss it. Decadal variability has been shown to be influenced among other factors by external natural forcing due to volcanoes (Church et al. 2005). During the estimation period, major volcanic eruptions occur in 1963 (Mount Agung), 1982 (El Chichon) and 1991 (Pinatubo). The first two eruptions are followed by few years coolings of both surface and subsurface integrated temperatures, especially marked in the Pacific basin. This is the region where the maximum cooling induced by volcanic aerosols occurs, as suggested by the coupled model study of Delworth et al. (2005). The impact of the

Pinatubo eruption on the Pacific SST is not as clear. The tropical Pacific SSTs are dominated by El Niño conditions between 1990 and 1995. The resulting warming seems to mask the effects due to volcanic forcing. On the contrary, the two integrated temperatures (Tiso14 and T250m) do show a cooling phase after 1991. In the subsurface, the main El Niño effect is in the same direction as the volcanic forcing. Indeed, in a large part of the equatorial Pacific basin, extending from West to the center, the isotherms move upwards (not shown), resulting in a subsurface cooling. At the basin scale, this cooling dominates the warming associated with the deepening thermocline in the eastern equatorial Pacific. The examination of the Diso14 time series shows no clear response to volcanic forcing. Consistent with Palmer and Haines (2009), this result confirms that isotherm depth changes are not sensitive to changes in air–sea heat flux.

Fig. 3 Time series of monthly anomalies of Tiso14, after a 5-year low-pass filter has been applied, as seen by EN3-OA (thick dotted black line), CERFACS, INGV, ECMWF and SODA. Each thin color line corresponds to the non-perturbed member of each individual reanalysis. The thick red line is the MEAN analysis, computed as the mean of SODA and the three ENSEMBLES reanalyses non-perturbed members. The standard deviation within the four time series used to compute the MEAN is indicated by the dotted brown line

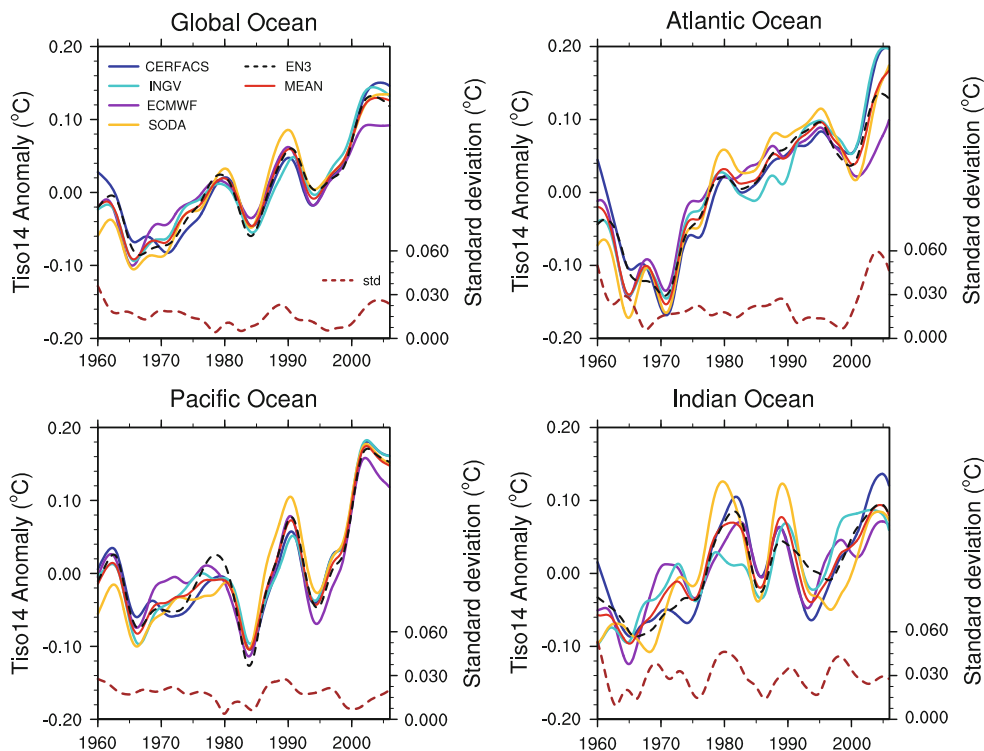


Fig. 4 Time series of the 5-year low-pass filtered monthly anomalies of SST (HadSST2), Tiso14, T250m and Diso14 as seen by the MEAN, ECMWF and ECMWF_update products. On the bottom-left panel, the three vertical lines indicate the timing of the major volcanic eruptions

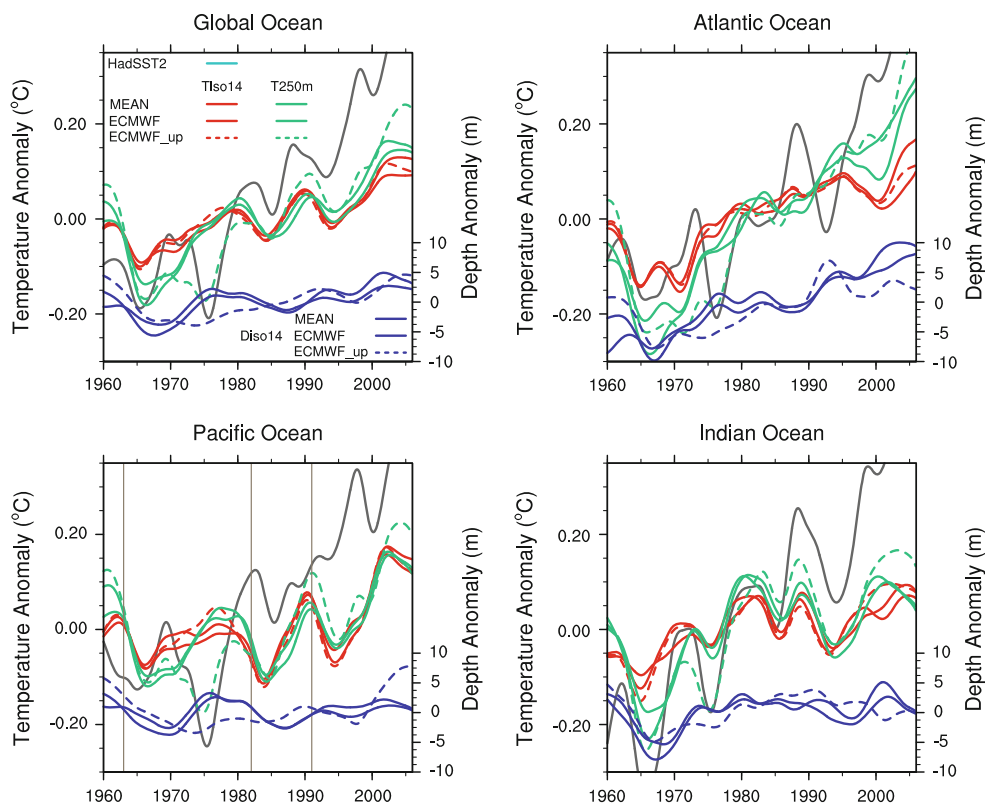


Table 3 Linear trend and amplitude of the decadal variability of the Tiso14 time series as seen by the MEAN (bold), EN3-OA, ECMWF and ECMWF_update products, over the period 1965–2005, in individual basins

Basins	Tiso14 trend (°C per decade)				Tiso14 decadal variability amplitude (°C)			
	EN3-OA	MEAN	ECMWF	ECMWF-update	EN3-OA	MEAN	ECMWF	ECMWF-update
Global	0.046	0.045 (+0.005, −0.010)	0.035	0.039	0.030	0.028 (+0.004, −0.002)	0.026	0.030
Atlantic	0.063	0.063 (+0.007, −0.016)	0.047	0.053	0.031	0.033 (+0.013, −0.001)	0.037	0.033
Pacific	0.046	0.047 (+0.009, −0.012)	0.035	0.035	0.053	0.048 (+0.007, −0.002)	0.055	0.063
Indian	0.033	0.026 (+0.007, −0.006)	0.020	0.032	0.036	0.039 (+0.022, −0.011)	0.036	0.040

To calculate the trends, the monthly Tiso14 anomalies have been averaged over each geographical basin. Then, a 5-year low-pass filter has been applied to each time-series. The trends correspond to the least square linear trend of each filtered time-series. The amplitude of the decadal variability is computed as the standard deviation of the detrended 5-year low-pass filtered Tiso14 time-series. Difference between the MEAN results and the maximum and minimum individual reanalyses results are indicated in brackets

Upper ocean temperature decadal variability may also result from internal ocean and/or coupled variability modes. The presence of large decadal fluctuations in the Pacific and Indian Ocean basins suggests an influence of El Niño Southern Oscillation (ENSO) and the Interdecadal Pacific Oscillation (IPO), on both SSTs and integrated variables. In agreement with Palmer et al. (2007), the T250m decadal variability is larger than that of Tiso14 (Tables 3, 4). It suggests that the use of Tiso14 increases the signal to noise ratio due to the filtering of dynamical changes associated with internal variability modes. The North Atlantic Oscillation (NAO) and Atlantic Multidecadal Oscillation (AMO) also play significant roles in the Atlantic basin. In particular,

the Diso14 deepening associated with T250m warming observed since 1980 may be related with predominantly positive phases in the NAO during this period (Palmer and Haines 2009). More recently, the AMO shift from negative to positive phase may also have reinforced those Atlantic trends. The spatial signature of the AMO and IPO modes on the three variables (Tiso14, T250m and Diso14) is investigated in Sect. 4.2.

Finally, a fraction of the decadal variability could also be artificial and induced by changes and/or biases in the observational datasets. In particular, the increased oceanic warming, occurring between 1970 and 1980, has been shown to be partly linked to a warm bias in XBT

temperature profiles (Gouretski and Koltermann 2007). Comparison between the ECMWF and ECMWF_update products allows us to quantify the XBT bias impact on the ocean heat content estimates. At the basin scale, the impact of the XBT correction on the amplitude of the decadal variability is weak (Tables 3, 4, 5). This is true in all the basins, and for the three variables. However, the specific details of the time evolution in T250m and Diso14 are strongly affected by the XBT correction especially during the 1970s and 1980s. We recall that the XBT bias has been attributed to erroneous reported depths of the profiles (Gouretski and Koltermann 2007). The bias thus affects isotherm depths directly. Understandably, the assimilation of data with the XBT correction of Wijffels et al. (2008) strongly impacts the evolution of Diso14. In particular, it suppresses the enhanced Diso14 deepening between 1970 and 1980, resulting in a damped Diso14 variability from 1970 to the late 1990s. The Diso14 weak variability exhibited by ECMWF_update in the Pacific basin confirms that there is no clear influence of volcanic forcing in the isotherm depth time series. As a result of the reduced Diso14 deepening, the XBT corrections also clearly modify the T250m time series. Whereas the T250m variable as seen by the ECMWF and MEAN products warms gradually between 1970 and 1980, ECMWF_update exhibits a strong cooling centered around 1975. Consistency between the T250m and SST is then increased and the strong SST cold episode during 1974–1976 in the Pacific and Indian Oceans also manifests itself in a reduced upper ocean heat content. Correlations between global T250m and SST time-series equal 0.85 and 0.97 when computed over the 1965–2005 period using ECMWF and ECMWF_update respectively. Between 1970 and 1980, the effect of the XBT corrections for Tiso14 opposes the one for T250m. At the global scale, the ECMWF_update anomalies in Tiso14 are slightly warmer than the ECMWF anomalies. This difference arises mainly from the Pacific basin. A possible mechanism for Tiso14 warming associated with Diso14 shallowing is related with an increased stratification which would reduce the vertical mixing and consequently warms the surface layers. Despite a few Tiso14 differences between ECMWF and ECMWF_update, the XBT corrections affect less this variable than the two others. This suggests that Tiso14 is relatively immune to the XBT bias even in the assimilation products.

The assimilation of XBT bias-corrected data also clearly affects the upper ocean evolution at the end of the estimation period. Whereas the effect on Diso14 varies from one basin to one other (shallowing in the Atlantic and Indian basins, and deepening in the Pacific basin), the corrections enhance the T250m warming after 2000 in all the basins. T250m warming associated with Diso14 shallowing may be the result of an increased warming near the

surface, together with an increased stratification at depth. However those results need to be taken with caution, as examination of local changes in Diso14 and T250m show that the spatial patterns are very contrasted (not shown). On the contrary, the effect of the XBT corrections between 1970 and 1980 is very consistent across different regions (not shown). Moreover, over the last decade, the effect of the XBT correction is mixed with the effect of altimeter data assimilation. Comparison between the MEAN and ECMWF curves suggests two effects of the introduction of altimeter data. First, Diso14 deepens inducing an enhanced T250m warming. This could be explained by a pushing down of the water column (i.e. a vertical displacement without any change in the stratification) resulting from the Cooper and Haines (1996) scheme used for assimilation of altimeter in the ECMWF system. This scheme translates sea level changes into vertical displacement of the water column (Vidard et al. 2009). Second, the warming in Tiso14 is reduced, which is not straightforward to understand. As the vertical displacement of the profiles by the assimilation of altimeter data is local in space and time, explaining the global effect (average in space and time) is not immediate. One possibility is that although in principle the altimeter only moves the water column up or down, the cumulated effect leads to additional vertical mixing, which might produce a stretching down of the water column (i.e. a vertical displacement leading to a reduced stratification). If the cold subsurface layers stretch more than the warm surface layers, it results in a Tiso14 cooling. This additional mixing may or may not be realistic. In order to confirm this hypothesis, we have compared the ECMWF product with an experiment based on the same model and assimilation system, but without altimeter data, as described in Balmaseda et al. (2007) (not shown). The comparison confirms that the assimilation of altimeter data indeed deepens the equatorial thermocline and cools the waters above the thermocline.

3.2 Linear trends

In terms of linear trends, the direct and fast response of SST to atmospheric changes results in a large warming trend of 0.14°C per decade at the global scale (Table 6). Understandably, due to the strong heat capacity of the ocean, the integrated Tiso14 and T250m trends exhibit smaller amplitudes. We first look at trends computed from analyses for which no XBT correction is applied. In all the basins, both T250m and Tiso14 EN3-OA trends are contained within the spread of the reanalyses trends (Table 3). Tiso14 is effective in filtering out the decadal variability, resulting in a trend analysis with larger signal to noise ratio than if using T250m, in all the basins. The trends in Tiso14 and T250m are of the same order of magnitude in the

Pacific and Indian basins. On the contrary, the trends in T250m almost double the trends in Tiso14 in the Atlantic basin (Tables 3, 4). For both EN3-0A and the reanalyses, the Atlantic T250m trend is a clear outlier whereas Tiso14 shows more uniform trends across the three ocean basins. This is consistent with Palmer et al. (2007) who explain the emergence of a spatially uniform Tiso14 trend by the reduction of the variability associated with local dynamical effects (at the basin scale). Indeed the strong T250m warming in the Atlantic basin is associated with marked Diso14 deepening (Table 5). For all the products, the global Diso14 deepening trends clearly arise from the Atlantic basin, while there are weak trends in the two other basins. The global Diso14 deepening found by Palmer and Haines (2009) is greater than one exhibited by EN3-OA. By far, this difference comes from the Atlantic trends, the one found by Palmer and Haines (2009) being about three times greater. As there is no infilling in the observations study of Palmer and Haines (2009), the well-sampled North Atlantic strongly influences their entire Atlantic and global-mean time series. Causes for the marked recent Diso14 deepening in the North Atlantic are investigated in Sect. 4. Interestingly, for the three variables, the Atlantic Ocean appears to be the basin with the strongest trend and weakest decadal variability, whereas the Indian Ocean is the basin with the strongest decadal variability and weakest trend.

ECMWF_update time series show that whereas the XBT corrections have little impact on the Tiso14 trend, it clearly increases the warming in T250m. Note however the strong dependence of the linear trend on the period chosen for the computations. Since the XBT correction induces a cooling period around 1965, it results in an increased linear trend when computed from 1965 to 2005. At the global scale, the T250m trend ranges from 0.070°C per decade (ECMWF) to 0.095°C per decade (ECMWF_update); i.e. a 34% increase. However, when computed over the 1960–2005 period, the ECMWF_update trend (0.067°C per decade) is only 24% larger than the ECMWF trend (0.054°C per decade). Another limitation of the trend calculation is to assume that the change is linear over time. Yet, Figs. 3 and 4 show that the upper ocean heat content time evolution varies among the different basins with an earlier warming of the Indian and Atlantic oceans. In the next section, we attempt to isolate the upper ocean temperature change due to anthropogenic forcing. Instead of using linear trend diagnostics, we use the regression methodology described in Sect. 2.3.

4 Causes and spatial patterns of upper-ocean temperature changes

Figure 5 illustrates the temporal pattern (denoted by μ) we use as index characterizing the response of the climate

system due to anthropogenic forcing. The μ patterns are computed, as described in Sect. 2.3, from nine CMIP3 AOGCMs. Over the whole period, the only external forcings prescribed to the selected AOGCMs are the anthropogenic ones. However, discrepancies between the models may arise from the range of anthropogenic forcings that are taken into account. In particular, the indirect effect of anthropogenic aerosols and the land use effect are not implemented by the same way in all AOGCMs. Such discrepancies probably explain a large part of the differences between the shapes of the curves shown Fig. 5. Nevertheless, the μ patterns obtained for each individual AOGCM all present the same general shape with a gradual warming culminating in a rapid increase of Tiso14 over the last 50 years. In the following, we only use the Multi-Model μ temporal pattern computed as the mean of the nine μ patterns obtained from individual CMIP3 AOGCMs. It shows a Tiso14 increase of 0.35°C over the whole period, with about plus 0.20°C occurring between 1965 and 2005.

4.1 Anthropogenically forced signal

Figures 6 and 7 illustrate the changes in Tiso14, T250m and Diso14, associated with the Multi-Model temporal pattern μ between 1965 and 2005. These figures are qualitatively consistent with Fig. 2 of Palmer et al. (2007) exhibiting linear trend maps. The spatial pattern for T250m changes presents common features with other fixed depth mean temperature analyses (Carton and Santorelli 2008; Bindoff et al. 2007). The Tropical Atlantic is dominated by a warming pattern, while the Pacific basin presents more contrasted changes with a warming in the subtropics and a cooling in the central and western equatorial regions. As noted by Palmer et al. (2007), T250m changes are related with changes in Diso14. In the Atlantic basin, the strong warming around 30°N is associated with isotherm deepening (Fig. 7), suggesting a net accumulation of heat in this region over the 1965–2005 period. In the Pacific basin, T250m cooling occurs with Diso14 shallowing, which indicates changes in both the east–west tilt and mean depth of the Pacific equatorial thermocline. In the ENSEMBLES reanalyses, these changes have been shown to be related with changes in the surface wind stress (Balmaseda et al. 2008a). In the western part of the basin, isotherm shallowing arises from a weakening of the equatorial easterlies over the last five decades. This is consistent with the observed reduction of the Walker circulation, related at least partially to anthropogenic forcing (Vecchi et al. 2006). This effect is combined with an off-equatorial intensification of the trades leading to increased divergence either side of the equator and increased convergence at around 15°N in the upper ocean. As a result, heat is

Table 4 Linear trend and amplitude of the decadal variability of the T250m time series, as seen by the MEAN (bold), EN3-OA, ECMWF and ECMWF_update products, over the period 1965–2005, in individual basins

Basins	T250m trend (°C per decade)				T250m decadal variability amplitude (°C)			
	EN3-OA	MEAN	ECMWF	ECMWF-update	EN3-OA	MEAN	ECMWF	ECMWF-update
Global	0.051	0.057	0.070	0.095	0.047	0.037	0.037	0.038
Atlantic	0.101	0.099	0.126	0.140	0.040	0.039	0.036	0.037
Pacific	0.036	0.045	0.049	0.077	0.062	0.049	0.055	0.054
Indian	0.037	0.041	0.052	0.082	0.070	0.066	0.067	0.071

Table 5 Linear trend and amplitude of the decadal variability of the Diso14 time series, as seen by the MEAN (bold), EN3-OA, ECMWF and ECMWF_update products, over the period 1965–2005, in individual basins

Basins	Diso14 trend (m per decade)				Diso14 decadal variability amplitude (m)			
	EN3-OA	MEAN	ECMWF	ECMWF-update	EN3-OA	MEAN	ECMWF	ECMWF-update
Global	0.57	1.03	2.05	1.88	1.52	1.43	1.46	1.00
Atlantic	2.85	3.23	4.37	3.05	1.64	1.49	1.60	1.88
Pacific	−0.11	0.17	0.89	1.55	1.55	1.60	1.67	2.00
Indian	0.45	0.90	1.83	1.20	2.23	1.99	2.36	1.91

Table 6 Linear trend and amplitude of the decadal variability of the SST time series computed from the HadSST2 dataset, over the period 1965–2005, in individual basins between 437.5°S and 37.5°N

Basins	SST trend (°C per decade)	SST decadal variability amplitude (°C)
Global	0.140	0.063
Atlantic	0.138	0.082
Pacific	0.133	0.072
Indian	0.154	0.080

exported from the equator towards 15°N/S. This effect appears clearly in the reanalyses which show maximum warming around 15°N/S, contrasting with the equatorial cooling. Results are somewhat different for the EN3-OA product which mostly exhibits T250m warming in the central equatorial Pacific area. However, EN3-OA does show significant marked warming around 15°N/S and is consistent with the reanalyses in terms of Diso14 change. In the central equatorial region, the observation coverage is very sparse before 1980 (Fig. 1). Whereas the analysis independent of any numerical model is thus strongly influenced by the climatology, the subsurface ocean temperature evolution as seen by the reanalyses is dynamically consistent with the changes in the surface wind stress. Consequently, we suggest that the central Pacific cooling exhibited by the reanalyses is robust. Nevertheless, the question remains whether the ERA-40 surface winds used to force both the ENSEMBLES and SODA reanalyses overestimate the recent changes in the tropical Pacific circulation. In the Indian Ocean, warming dominates,

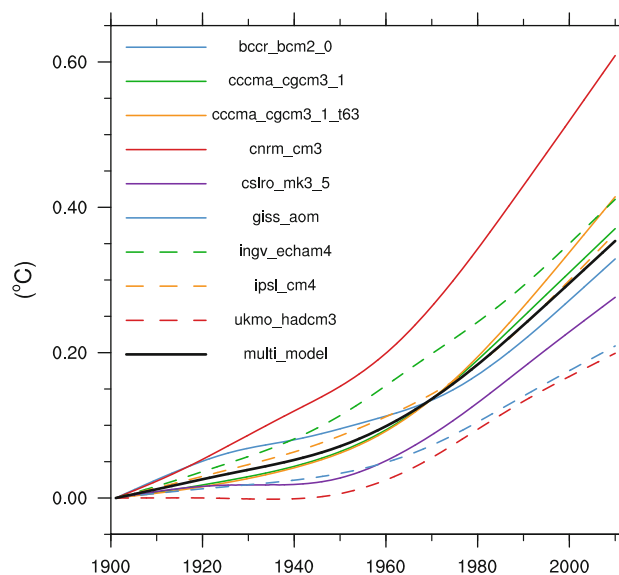


Fig. 5 Temporal pattern μ evaluated from the CMIP3 models. The figure represents the obtained smooth patterns as a function of time, using the year 1901 as a reference

except around 10°S where T250m cooling is produced by mechanisms similar to those described in the Pacific basin (Balmaseda et al. 2008a). The SODA product exhibits the widest cooling zone. Carton and Santorelli (2008) have already noticed that this reanalysis shows a very pronounced cold anomalies in the eastern part of the Indian basin. Figure 6 shows that the SODA T250m cooling is linked with a particularly marked isotherm deepening in the Indian Ocean. Differences between the SODA and others reanalyses changes are reduced for Tiso14.

In general, the spatial structure of the Tiso14 changes is smoother than the spatial structure in T250m and Diso14, shows more uniform pattern, and seems more consistent between reanalysis products. The spatial patterns of T250m and Diso14 are more complex, since they are affected by local heat storage and redistribution of heat due to changes in the ocean circulation. The dispersion among reanalyses is larger in these two variables. Although the cooling in the equatorial Pacific and southern Indian oceans appears to be robust, there is some uncertainty about its magnitude and the east–west gradients. In the Atlantic basin, the ECMWF and ECMWF_updated reanalyses exhibit stronger T250m warming and Diso14 deepening than other products. This result may suggest that the warming is penetrating deeper over time, and so causing the depth of the 14°C isotherm to increase. This may be due to the weaker relaxation to climatology used in the ECMWF reanalyses. Another possibility is that the strong changes in T250m and Diso14 shown by those two products are linked with the introduction of altimeter data which pushes down the water column. Spatial correlations between the change in Diso14 and the pattern of the differences in changes between Tiso14 and T250m (not shown) are indicated in Fig. 7. Most of them are in the range 0.6–0.7, smaller than the 0.77 correlation found by Palmer et al. (2007). The difference between Tiso14 and T250m trends, together with the resemblance between T250m and Diso14, would suggest that changes in the upper ocean heat content can not be explained without considering changes in the global ocean circulation. Finally, the strong similarity between the Tiso14 change patterns as seen by ECMWF and ECMWF_updated confirms that Tiso14 is not very sensitive to the XBT bias. Impact of the XBT corrections is more noticeable in T250m change maps. For example, the ECMWF_update change map exhibits more intense warming around 10°N in the Atlantic and in the eastern Pacific basins. Note however that in general, the two analyses show very similar patterns of change. A possible explanation is that the corrections are mostly applied as a function only of depth and time (Wijffels et al. 2008) and thus have a small impact on the local changes. This result is consistent with Carson and Harrison (2010) who find that the strength and spatial patterns of regional interdecadal variability, at the sub-basin to basin scales, are unaffected by the application of bias correction to the XBT fall rates.

4.2 Signature of internal variability modes

Once the anthropogenic forced signal has been isolated, we can interpret the residual as an estimate of the recent upper ocean temperature internal variability. Here we choose to focus on the signature of the two following low-frequency internal modes: the Interdecadal Pacific Oscillation (IPO)

(Power et al. 1999), in the Pacific and Indian Ocean basins and the Atlantic Multidecadal Oscillation (AMO) (Kerr 2000) in the Atlantic Ocean. The IPO index corresponds to the standardized PC time series associated with the first EOF of the SST internal variability in the Pacific basin between 40°S and 60°N. The AMO index is the standardized time series of the area weighted SST internal variability in the Atlantic basin between 0° and 60°N. SST data are from the ERSST2 dataset (Reynolds et al. 2002). To compute internal variability, we first constructed a CMIP3 Multi-Model temporal pattern characterizing the response of the SST to anthropogenic forcing. This pattern is obtained by applying the procedure described in Sect. 2.3 to the global 10-year low-pass filtered monthly SST from the nine CMIP3 AOGCMs listed Table 2, and by averaging the nine resulting curves. The regression of the observed SST on this temporal pattern can be considered as an estimate of the SST spatial change associated with the anthropogenic forcing. The SST internal variability we use here corresponds to the regression residual.

The IPO explains about 30% of the total variance of the internally varying SST in the Pacific basin between 1901 and 2009 (not shown). The north Pacific part of the pattern is known as the Pacific Decadal Oscillation (Mantua et al. 1997). Over the whole period, the IPO index exhibits multi-decadal oscillations (Fig. 8). Between 1965 and 2005, we note two sharp transitions from negative to positive phase in the mid-1970s (transition often referred to as the 1976 Pacific climate shift), and from positive to negative phase around 2000. In the North Atlantic basin, SST also displays internal variability on multi-decadal time scales. The AMO index exhibits cold anomalies during the periods 1900–1920 and 1970–1990 with an intervening warmer period during 1940–1960. Over the period of interest (1965–2005), the AMO index is mainly negative and transitions to positive phase in 2000.

During positive phases of the IPO, the three variables (Tiso14, T250m and Diso14) exhibit a meridional tripole structure very similar between all products (Fig. 9). In the eastern part of the tropical Pacific and in the western and central Indian Ocean, Diso14 deepens which induces accumulation of heat leading to warm T250m anomalies. On the contrary, around the Maritime Continent, isotherms shallow, leading to cold T250m anomalies. In the Pacific basin, the IPO then entails thermocline vertical displacements which are captured by the T250m variable. The IPO spatial signature in T250m is very similar to the one in SST described in several studies (e.g. Power et al. 1999; Parker et al. 2007; Meehl et al. 2009). It is interesting to compare changes in the Pacific equatorial thermocline depth due to anthropogenic forcing and due to the IPO mode. The former mostly exhibit uniform zonal structure with Diso14 deepening in subtropical regions and shallowing at the

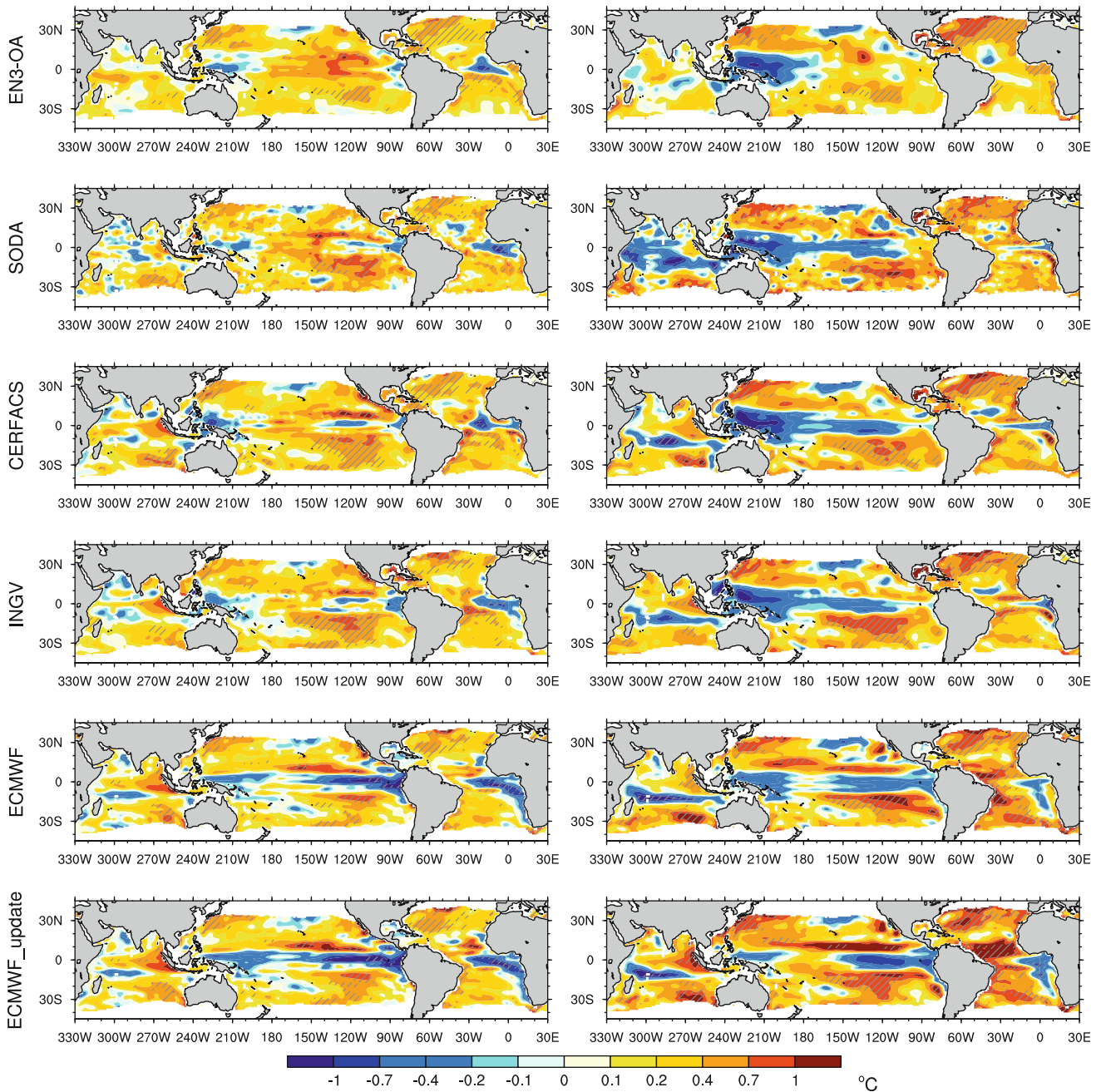


Fig. 6 Changes (δ in $^{\circ}\text{C}$) in Tiso14 (left) and T250m (right) associated with the Multi-model μ temporal pattern, as seen by EN3-OA, SODA, CERFACS, INGV, ECMWF, and ECMWF_update, estimated over the 1965–2005 period. A simple nine point local smoothing has been applied to remove some of the grid-scale noise.

Gray hatching indicates that the regression is significantly different from zero at the 95% level [Student’s t test with six degrees of freedom, corresponding to the number of months (492) divided by the cutoff frequency of the filter (60) minus two]

equator, except off the American coast. The latter present opposite behavior in the western and eastern part of the Pacific basin, associated with fluctuations in the east–west tilt of the thermocline (with a reduction of the mean tilt during the IPO positive phase). Consequently, the T250m changes related to the IPO oppose the ones related to anthropogenic forcing in the western subtropical regions

and along the equator, between 150°W and 120°W (with the exception of the EN3-OA dataset which does not show any central Pacific equatorial cooling, as commented previously). In the rest of the Pacific basin, similar changes (in terms of sign) arise from the IPO and the anthropogenically forced response. Such a similarity has already been suggested by Meehl et al. (2009) who identify elements of the

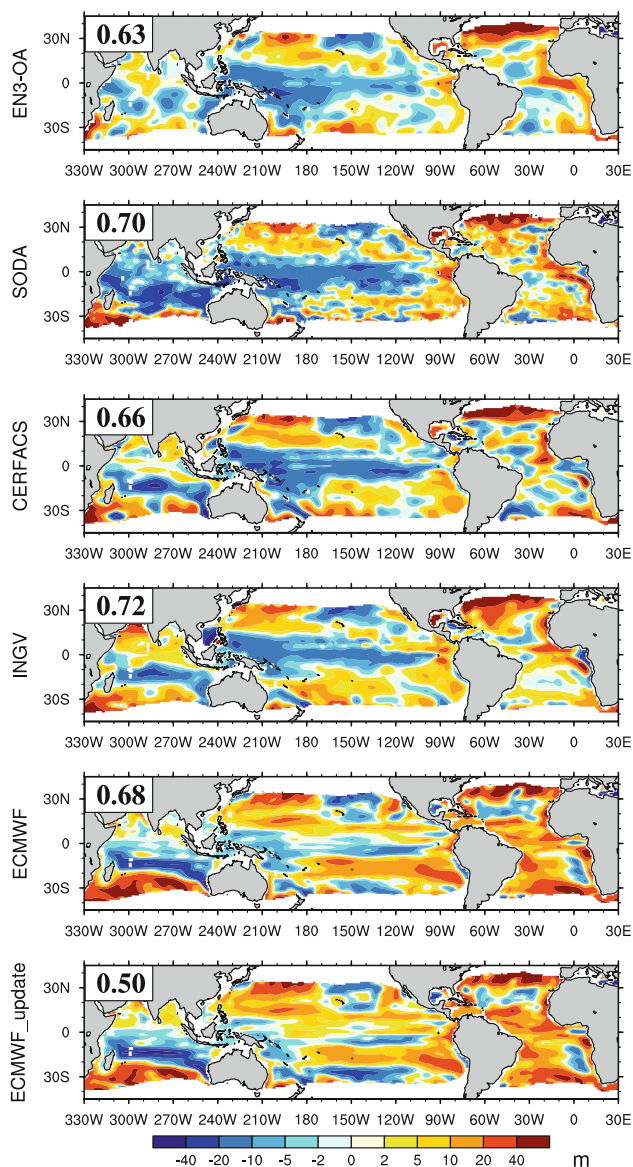


Fig. 7 Changes (δ in m) in the 14°C isotherm depth associated the Multi-model μ temporal pattern, as seen by EN3-OA, SODA, CERFACS, INGV, ECMWF, and ECMWF_update, estimated over the 1965–2005 period. A simple nine point local smoothing has been applied to remove some of the grid-scale noise. Spatial correlations between the change in Diso14 and the pattern of the differences in changes between Tiso14 and T250m are indicated for each product

SST IPO pattern present in both forced and unforced simulations from a coupled global climate model. While the sign of Tiso14 anomalies associated with the IPO signature is very consistent with the one of T250m anomalies, the intensity is clearly reduced. This result again illustrates the Tiso14 ability to filter out dynamical effects. Differences between the IPO signature as seen by the different products are not significant for Tiso14. In particular, no impact of the XBT correction is visible and we notice no discrepancy between the two reanalyses which assimilate

altimeter data and the other products. The T250m spatial structures associated with the IPO are also very similar to each other, but the amplitude of the T250m anomalies slightly varies between products. It seems that the XBT correction enhances the T250m warm anomalies in the eastern Pacific basin.

In the Atlantic basin, strong T250m anomalies associated with the AMO index (Fig. 10) are also shown by ECMWF_update. This is not surprising, as the AMO index is computed from SST which is not prone to XBT bias. The similarity between the surface and sub-surface is then reinforced in the reanalysis which assimilates corrected profiles. A similar result has already been noted in Fig. 4. Reduction of Tiso14 anomalies associated with the AMO mode, compared with T250m anomalies is not as clear as for the IPO mode. It is probably because the dynamical link between vertical isotherm motions and the AMO mode is not as clear as it is with the IPO mode. The comparison of Tiso14 and T250m spatial patterns associated with the AMO reveals significant discrepancies. For example, in the central Atlantic basin, between 10° and 15°N, the EN3-OA product shows warm Tiso14 anomalies contrasting with cold T250m anomalies. Despite differences among products and variables, the AMO signature in the upper ocean roughly displays cold anomalies in the south-western and north-western parts of the basin, as well as around the equator. Warm anomalies appear along the African coast, extending westwards around 10°S, and in a large band from Morocco to the Caribbean sea. In the Northern Hemisphere, opposite patterns between the eastern and western regions may be related to the westward propagation of subsurface temperature anomalies associated with the AMO, as noted by Frankcombe et al. (2008). While a new anomaly is spreading in the north tropical eastern Atlantic basin, an anomaly of opposite sign from the previous oscillation phase would remain in the north-western part of the basin. While in terms of SST, the AMO and anthropogenic signature are both dominated by a widespread warming in the North Atlantic basin (Kerr 2000), the subsurface AMO signature clearly differs from the one of anthropogenic changes. Note the exceptions of the eastern and central subtropics of the North Atlantic ocean where both signatures show a recent warming of the upper ocean associated with isotherm deepening. This result is consistent with the ocean model study of Marsh et al. (2008) which concludes that the recent warming in the North Atlantic basin is both related to net surface heat fluxes and to ocean advection of heat, the latter been closely associated with the Atlantic Meridional Ocean Circulation (AMOC) variability in the tropical and subtropical regions. Joint variability in the strength of the AMOC and an AMO-like pattern of surface temperature variability has previously been demonstrated in the coupled ocean-atmosphere

Fig. 8 Time series of the IPO index (left) and the AMO index (right) from 1901 to 2009

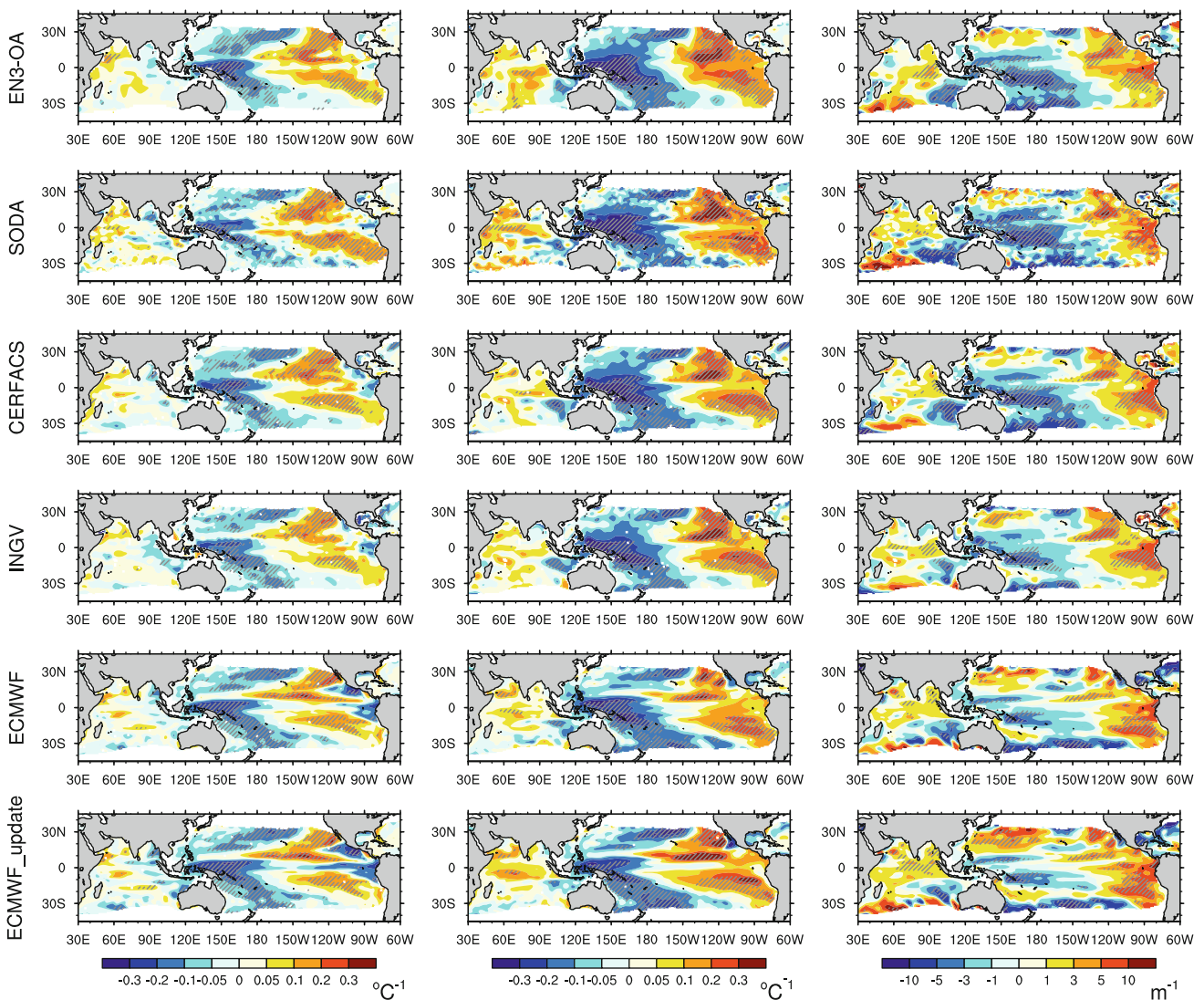
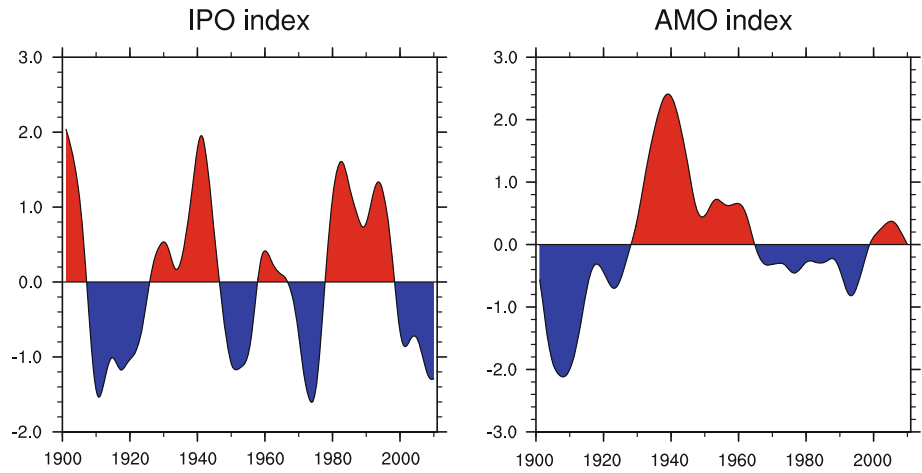


Fig. 9 Regression of the internal variability of the 5-year low-pass filtered monthly anomalies of Tiso14 (left), T250m (center) and Diso14 (right), on the IPO index, as seen by EN3-OA, SODA, CERFACS, INGV, ECMWF, and ECMWF_update, computed over

the 1965–2005 period. A simple nine point local smoothing has been applied to remove some of the grid-scale noise. Gray hatching indicates that the regression is significantly different from zero at the 95% level (Student's *t* test with six degrees of freedom)

model study of Knight et al. (2005). The latter, consistent with previous studies (e.g. Enfield et al. 2001), also suggested that the AMO is currently at or near a peak and likely to diminish thereafter (Knight et al. 2005), thus partially offsetting expected Northern Hemisphere warming. On the contrary, our AMO index (together with other studies; e.g. Trenberth and Shea 2006; Parker et al. 2007; Ting et al. 2009), suggests that positive phase of the AMO has just started over the last years. The AMO may thus reaches its peak amplitude in the coming years, increasing even further north Atlantic upper ocean warming. Differences in the temporal properties of the AMO index arise from the method used to remove the influence of global warming. Whereas the former studies remove a local linear trend from the data, the others use larger-scale global signals as proxy for the anthropogenically forced signal.

5 Summary and conclusions

This paper has examined the recent evolution of the mean temperature above the 14°C isotherm in the global ocean, as viewed by five model-based reanalyses and a model-independent objective analysis. The most recent reanalysis assimilates data with new time-varying XBT bias corrections Wijffels et al. (2008). We define the MEAN reanalysis as the average of the four other reanalyses, whose global spread is always lower than 0.04°C. Over the 1965–2005 period, the MEAN reanalysis exhibits a global warming trend of 0.045°C per decade superimposed with decadal variability of 0.028°C standard deviation. Results are very similar for the model-independent objective analysis with a global trend of 0.046°C per decade and decadal variability of 0.030°C standard deviation. In all the basins, the trend of the objective analysis is contained within the spread of the reanalyses trends. Spatially, estimated change associated with anthropogenic forcing is largely dominated by a warming pattern. For most products, cooling zones are limited to small patches in the equatorial band, in the central Pacific around 30°N, and along the African west coast. In a few regions, the anthropogenically forced signal may have been reinforced by internal variability associated with the AMO and IPO. In the Pacific basin (in the western equatorial region and in an area centered around 30°N and 140°W,) both IPO and anthropogenic related changes exhibit cooling patterns. On the contrary, both contributions lead to upper ocean warming in the southern subtropical Pacific. In the North Atlantic basin, the positive AMO phase may also have reinforced the recent warming. With the exception of those regions, the signature of the AMO and IPO internal variability modes differs clearly from the anthropogenically forced signal. The question remains whether there are other

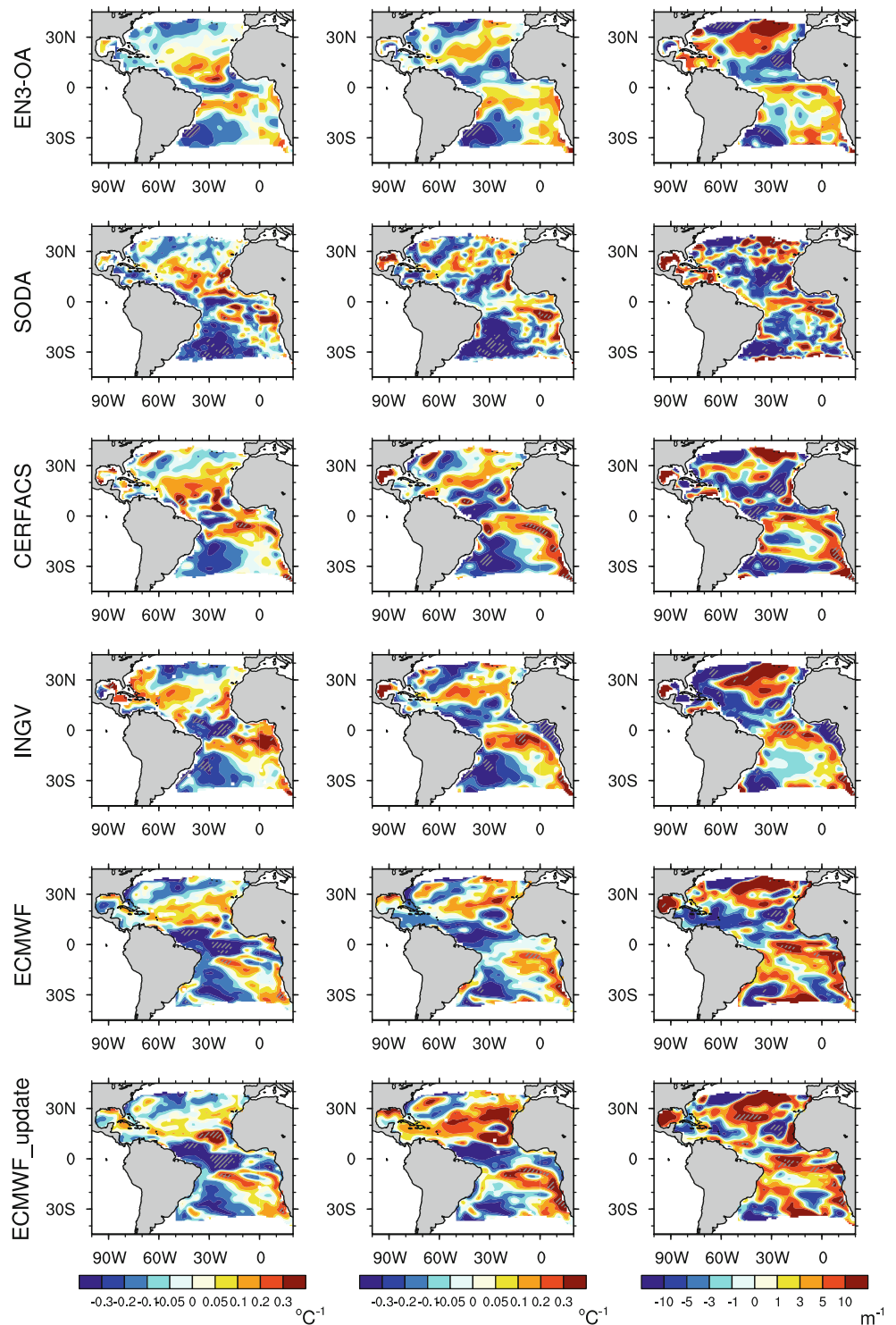
important internal decadal variability modes not included in this analysis which can project onto the signature of the long-term changes.

The recent evolution of Tiso14 has been compared with the one of the 250 m mean temperature. Two major advantages of the Tiso14 analysis have been emphasized. First, it filters out temperature change due to vertical isotherm motion, associated both with internal variability and anthropogenic forcing. In the Pacific basin, internally varying isotherm depths are related to the IPO induced fluctuations in the east–west tilt of the thermocline. Anthropogenically forced isotherm motions result in long-term shallowing in the western and central equatorial Pacific and around 10°S in the Indian Ocean. On the contrary, isotherms deepen in the North Atlantic basin, suggesting a net accumulation of heat water in this region. The water balance between the Indian and Pacific low latitudes on the one hand, and the North Atlantic on the other hand may be related to changes in the AMOC (Palmer and Haines 2009). However, our 40-year period of study is too short to draw confident conclusions linked with the global ocean circulation on secular time scales and to determine whether the long-term circulation changes are wind or thermo-haline driven.

The second advantage of Tiso14 is that it is not very sensitive to the XBT bias fall-rate. Our results show that the impact of the XBT's bias on the spatial pattern of change is quite weak. On the contrary, this bias is a major source of uncertainty for the time evolution of a mean temperature above a fixed depth. The main impact of the XBT correction is the suppression of the accentuated warming between 1970 and 1980, inducing a 34% increase in the T250m trend computed over 1965–2005. Our result is consistent with Domingues et al. (2008) who examine the ocean upper 300 m in an objective analysis based on the EN3 profiles after applying the correction by Wijffels et al. (2008). They found an ocean warming trend about 50% larger than previous estimates (Levitus et al. 2005). Nevertheless, other groups obtain different results using different XBT bias corrections (Ishii and Kimoto 2008; Levitus et al. 2009). The main difficulty in resolving the XBT bias seems to be the lack of accurate metadata, with approximately half of XBTs being of unknown type (Palmer et al. 2010). Research is still underway to establish a consensual correction.

Beyond the issue of the XBT bias, the intercomparison of different ocean analyses allows us to identify other uncertainties associated with the recent upper ocean temperature evolution. The consistency between the observations and the reanalyses results, as well as the spread among the reanalyses, has been used as a simple estimate of ocean state uncertainties. We found that at the end of the estimation period, introduction of altimeter data within the

Fig. 10 Regression of the internal variability of the 5-year low-pass filtered monthly anomalies of Tiso14 (left), T250m (center) and Diso14 (right), on the AMO index, as seen by EN3-OA, SODA, CERFACS, INGV, ECMWF, and ECMWF_update, computed over the 1965–2005 period. A simple nine point local smoothing has been applied to remove some of the grid-scale noise. Gray hatching indicates that the regression is significantly different from zero at the 95% level (Student’s *t* test with six degrees of freedom)



assimilation scheme is responsible for the ECMWF divergence from the other ENSEMBLES reanalyses. Although it is clear that altimeter assimilation has a noticeable effect in the ocean heat thermal structure, and therefore in the representation of ocean heat content trends, it is not easy to say if it produces a more reliable estimation. Therefore, the impact of assimilation on the ocean

heat content signals deserves more attention. We would like to underline the limits of such an intercomparison exercise. When possible, we have attempted to propose reasons for the origin of the discrepancies. However, identifying the detailed causes remains difficult. Indeed, many factors can be involved such as model errors, problems associated with the assimilation systems and/or with

the atmospheric forcings, biases and scarcity of the observations. Within the ENSEMBLES reanalyses, while the atmospheric forcing fields and the assimilated observations used are the same, the number of possible causes for discrepancies is reduced. Nevertheless, their clear understanding would require additional intercomparison studies currently planned within the Climate Variability and Predictability (CLIVAR) Global Synthesis and Observations Panel (GSOP) (Stammer 2006).

In general, the results presented here on the comparison of Tiso14, T250m and Diso14 support the findings of Palmer et al. (2007). The use of reanalyses, as a dynamically based means of combining the in situ observations with the best available estimates of forcing fields, makes it possible to extend the Tiso14 analysis in the data sparse region. Moreover, we argue that the regression based method presented here allows an optimal separation of the anthropogenically forced changes from internal variability. Future work will require determining whether the temporal pattern characterizing the anthropogenic climate change (μ) is significantly contained in the observations and reanalyses, by using a statistical test developed by Ribes et al. (2009). This next step will constitute a detection study of climate change in the upper ocean. In order to carry out the detection study on a larger latitude domain, careful examination of the appropriate variable to examine will be needed. For example, using the temperature integrated throughout the mixed layer depth could present the same advantage as Tiso14 as a dynamical filter, but without the need to exclude the high latitudes.

Acknowledgments The ENSEMBLES data used in this work was funded by the EU FP6 Integrated Project ENSEMBLES (contract number 505539) whose support is gratefully acknowledged. In particular, the authors thank Philippe Rogel for his assistance and advice with the reanalyses. The SODA data were obtained from the IRI/LDEO Climate Data Library Web site (<http://ingrid.ldeo.columbia.edu/SOURCES/CARTON-GIESE/SODA/v2p0p2-4/>). We are very grateful to Simon Good who provided the EN3_v2a version of the ENACT/ENSEMBLES quality-controlled dataset, and Matthew Palmer who provided the code we used to filter the data. We acknowledge the modeling groups, the Program for Climate Model Diagnosis and Intercomparison (PCMDI) and the WCRP's Working Group on Coupled Modelling (WGCM) for their roles in making available the WCRP CMIP3 multi-model dataset. Support of this dataset is provided by the Office of Science, U.S. Department of Energy. We thank Gilles Reverdin, Thierry Delcroix, Sophie Cravatte and Gael Alory for stimulating discussions on this work, and anonymous reviewers whose comments helped to improve this manuscript. The figures were produced with the NCL software developed at NCAR.

References

- AchutaRao K, Ishii M, Santer B, Gleckler P, Taylor K, Barnett T, Pierce D, Stouffer R, Wigley T (2007) Simulated and observed variability in ocean temperature and heat content. *Proc Natl Acad Sci* 104:10768–10773
- Adler RF, Huffman GJ, Chang A, Ferraro R, Xie P, Janowiak J, Rudolf B, Schneider U, Curtis S, Bolvin D, Gruber A, Susskind J, Arkin P, Nelkin E (2003) The Version-2 Global Precipitation Climatology Project (GPCP) monthly precipitation analysis (1979–present). *J Hydrometeorol* 4:1147–1167
- Balmaseda M, Anderson D, Vidard A (2007) Impact of argo on analyses of the global ocean. *Geophys Res Lett* 34:L16605. doi: [10.1029/2007GL030452](https://doi.org/10.1029/2007GL030452)
- Balmaseda M, Anderson D, Molteni F (2008a) Climate variability from the New ECMWF Ocean Reanalysis ORA-S3. Third WCRP international conference on reanalysis. <http://wcrp.ipsl.jussieu.fr/Workshops/Reanalysis2008/abstract.html>
- Balmaseda M, Vidard A, Anderson D (2008b) The ECMWF ocean analysis system ORA-S3. *Mon Wea Rev* 136:3018–3034
- Banks H, Wood R (2002) Where to look for anthropogenic climate change in the ocean. *J Clim* 15:879–891
- Barnett T, Pierce D, AchutaRao K, Gleckler P, Santer B, Gregory J, Washington W (2005) Penetration of human-induced warming into the world's oceans. *Sci Agric* 309:284–287
- Bellucci A, Masina S, Pietro PD, Navarra A (2007) Using temperature–salinity relations in a global ocean implementation of a multivariate data assimilation scheme. *Mon Wea Rev* 135:3785–3807
- Bindoff N, Willebrand J, Artale V, Cazenave A, Gregory J, Gulev S, Hanawa K, Qiu CL, Levitus S, Nojiri Y, Shum C, Talley L, Unnikrishnan A (2007) Observations: oceanic climate change and sea level. In: Solomon S, Qin D, Manning M, Chen Z, Marquis M, Averyt KB, Tignor M, Miller HL (eds) *Climate change 2007: the physical science basis. Contribution of working group I to the fourth assessment report of the intergovernmental panel on climate change*. Cambridge University Press, Cambridge, United Kingdom and New York, NY, USA
- Boyer T, Stephens C, Antonov J, Conkright M, Locarnini R, O'Brien T, Garcia H (2002) *World Ocean Atlas 2001*. In: Levitus (ed) *Salinity, NOAA Atlas NESDIS 50, vol 2*. U.S. Govt. Print. Off., Washington, DC, 176 pp
- Carson M, Harrison D (2010) Regional interdecadal variability in bias-corrected ocean temperature data. *J Clim* 23:2847–2855
- Carton J, Giese B (2008) A reanalysis of Ocean Climate Using Simple Ocean Data Assimilation (SODA). *Mon Wea Rev* 136:2999–3017
- Carton J, Santorelli A (2008) Global decadal upper-ocean heat content as viewed in nine analyses. *J Clim* 21:6015–6035
- Church J, White N, Arblaster J (2005) Significant decadal-scale impact of volcanic eruptions on sea level and ocean heat content. *Nat Biotechnol* 438:74–77
- Cooper M, Haines K (1996) Data assimilation with water property conservation. *J Geophys Res* 101(C1):1059–1077
- Daget N, Weaver A, Balmaseda M (2009) Ensemble estimation of background-error variances in a three-dimensional variational data assimilation system for the global ocean. *Q J R Meteorol Soc* 135:1071–1094
- Davey M, Huddleston M, Ingleby B, Haines K, Le Traon P, Weaver A, Vialard J, Anderson D, Troccoli A, Vidard A, Burgers G, Leeuwenburgh O, Bellucci A, Masina S, Bertino L, Korn P (2006) Multi-model multi-method multi-decadal ocean analyses from the ENACT project. *CLIVAR Exch* 11:22–25
- De Mey P, Benkiran M (2002) A multivariate reduced-order optimal interpolation method and its application to the Mediterranean basin-scale circulation. In: Pinardi N, Woods JD (eds) *Ocean forecasting: conceptual basis and applications*. Springer, New York

- Delworth T, Ramaswamy V, Stenchikov G (2005) The impact of aerosols on simulated ocean temperature and heat content in the 20th century. *Geophys Res Lett* 32:L24709. doi:[10.1029/2005GL024457](https://doi.org/10.1029/2005GL024457)
- Domingues CM, Church JA, White NJ, Gleckler PJ, Wijffels SE, Barker PM, Dunn JR (2008) Improved estimates of upper-ocean warming and multi-decadal sea-level rise. *Nat Biotechnol* 453:1090–1094
- Enfield D, Mestas-Nunez A, Trimble P et al (2001) The Atlantic multidecadal oscillation and its relation to rainfall and river flows in the continental U.S. *Geophys. Res Lett* 28:2077–2080
- Frankcombe L, Dijkstra H, von der Heydt A (2008) Sub-surface signatures of the Atlantic Multidecadal Oscillation. *Geophys Res Lett* 35:L19602
- Gouretski V, Koltermann K (2007) How much is the ocean really warming?. *Geophys Res Lett* 34:L01610. doi:[10.1029/2006GL027834](https://doi.org/10.1029/2006GL027834)
- Hanawa K, Rual P, Bailey R, Sy A, Szabados M (1995) A new depth-time equation for sippican or tsk t-7, t-6 and t-4 expendable bathythermographs (xbt). *Deep Sea Res I* 42:1423–1451
- Hegerl G, Zwiers FW, Braconnot P, Gillett N, Luo Y, Orsini JM, Nicholls N, Penner J, Stott P (2007) Understanding and attributing climate change. In: Solomon S, Qin D, Manning M, Chen Z, Marquis M, Averyt KB, Tignor M, Miller HL (eds) *Climate change 2007: the physical science basis. Contribution of working group I to the fourth assessment report of the intergovernmental panel on climate change*. Cambridge University Press, Cambridge, United Kingdom and New York, NY, USA
- Ingleby B, Huddleston M (2007) Quality control of ocean temperature and salinity profiles—historical and real-time data. *J. Mar. Syst.* 65:158–175
- Ishii M, Kimoto M (2009) Reevaluation of historical ocean heat content variations with time-varying xbt and mbt depth bias. *J Oceanogr* 65:287–299. doi:[10.1007/s10872-009-0027-7](https://doi.org/10.1007/s10872-009-0027-7)
- Ishii M, Kimoto M, Kachi M (2003) Historical ocean subsurface temperature analysis with error estimates. *Mon Wea Rev* 131:51–73
- Kerr R (2000) A North Atlantic climate pacemaker for the centuries. *Sci Agric* 288:1984
- Kizu S, Yoritaka H, Hanawa K (2005) A new fall-rate equation for T-5 expendable bathythermograph (XBT) by TSK. *J Oceanogr* 61:115–121
- Knight JR, Allan RJ, Folland CK, Vellinga M, Mann ME (2005) A signature of persistent natural thermohaline circulation cycles in observed climate. *Geophys Res Lett* 32:L20708. doi:[10.1029/2005GL024233](https://doi.org/10.1029/2005GL024233)
- Knight J, Folland C, Scaife A (2006) Climate impacts of the Atlantic multidecadal oscillation. *Geophys Res Lett* 33:L17706
- Le Traon P, Nadal F, Ducet N (1998) An improved mapping method of multisatellite altimeter data. *J Atmos Ocean Technol* 15:522–534
- Levitus S, Antonov J, Boyer T (2005) Warming of the world ocean, 1955–2003. *Geophys Res Lett* 32:L02604. doi:[10.1029/2004GL021592](https://doi.org/10.1029/2004GL021592)
- Levitus S, Antonov J, Boyer T, Locarnini R, Garcia H, Mishonov AV (2009) Global ocean heat content 1955–2008 in light of recently revealed instrumentation problems. *Geophys Res Lett* 36:L07608. doi:[10.1029/2008GL037155](https://doi.org/10.1029/2008GL037155)
- Lyman J, Good S, Gouretski V, Ishii M, Johnson G, Palmer M, Smith D, Willis J (2010) Robust warming of the global upper ocean. *Nat Biotechnol* 465:334–337
- Madec G, Delecluse P, Imbard M, Levy C (1998) OPA 8.1 Ocean General Circulation Model reference manual. Notes du pôle modélisation, Institut Pierre Simon Laplace(IPSL), France
- Mann M, Emanuel K (2006) Atlantic hurricane trends linked to climate change. *Eos* 87:233–244
- Mantua N, Hare S, Zhang Y, Wallace J, Francis R (1997) A pacific interdecadal climate oscillation with impacts on salmon production. *Bull Am Meteorol Soc* 78:1069–1079
- Marsh R, Josey S, De Cuevas B, Redbourn L, Quartly G (2008) Mechanisms for recent warming of the North Atlantic: Insights gained with an eddy-permitting model. *J Geophys Res* 113:C04031. doi:[10.1029/2007JC004096](https://doi.org/10.1029/2007JC004096)
- Meehl G, Hu A, Santer B (2009) The mid-1970s climate shift in the Pacific and the relative roles of forced versus inherent decadal variability. *J Clim* 22:780–792. doi:[10.1175/2008JCLI2552.1](https://doi.org/10.1175/2008JCLI2552.1)
- Murphy J, Collins M, Doblas-Reyes F, Palmer T (2009) Development of ensemble prediction systems volume ENSEMBLE: climate change and its impacts: summary of research and results from the ENSEMBLE project. In: van der Linden P, Mitchell JFB (eds) *Met Office Hadley Centre. FitzRoy Road, Exeter EX1 3PB, UK*, 160 pp
- Palmer M, Antonov J, Barker P, Bindoff N, Boyer T, Carson M, Domingues C, Gille S, Gleckler P, Good S et al (2010) Future observations for monitoring global ocean heat content. *Proc OceanObs* 9:21–25
- Palmer M, Good S, Haines K, Rayner N, Stott P (2009) A new perspective on warming of the global ocean. *Geophys Res Lett* 36:L20709. doi:[10.1029/2009GL039491](https://doi.org/10.1029/2009GL039491)
- Palmer M, Haines K (2009) Estimating oceanic heat content change using isotherms. *J Clim* 22:4953–4969
- Palmer M, Haines K, Tett S, Ansell T (2007) Isolating the signal of ocean global warming. *Geophys Res Lett* 34:L23,610
- Parker D, Folland C, Scaife A, Knight J, Colman A, Baines P, Dong B (2007) Decadal to multidecadal variability and the climate change background. *J Geophys Res* 112:D18115. doi:[10.1029/2007JD008411](https://doi.org/10.1029/2007JD008411)
- Power S, Casey T, Folland C, Colman A, Mehta V (1999) Interdecadal modulation of the impact of ENSO on Australia. *Clim Dyn* 15:319–324
- Rayner N, Brohan P, Parker D, Folland C, Kennedy J, Vanicek M, Ansell T, Tett S (2006) Improved analyses of changes and uncertainties in sea surface temperature measured in situ since the mid-nineteenth century: the HadSST2 dataset. *J Clim* 19:446–469
- Reynolds R, Rayner N, Smith T, Stokes D, Wang W (2002) An improved in situ and satellite SST analysis for climate. *J Clim* 15:1609–1625
- Ribes A, Azaïs J, Planton S (2009) A method for regional climate change detection using smooth temporal patterns. *Clim Dyn* 1–16. doi:[10.1007/s00382-009-0670-0](https://doi.org/10.1007/s00382-009-0670-0)
- Smith R, Dukowicz J, Malone R (1992) Parallel ocean general circulation modeling. *Phys D* 60:38–61
- Stammer D (2006) Report of the 1st CLIVAR workshop on ocean reanalysis, 8–10 November 2004, Boulder USA. ICPO Publication Series 93 WCRP Informal Publication 9/2006
- Stephens C, Antonov J, Boyer T, Conkright M, Locarnini R, O'Brien T, Garcia H (2002) World Ocean Atlas 2001, vol 1: Temperature. In: Levitus S (ed) *NOAA Atlas NESDIS 49*. U.S. Government Printing Office, Washington, DC
- Sutton R, Hodson D (2005) Atlantic Ocean forcing of North American and European summer climate. *Sci Agric* 309:115
- Thadathil P, Saran A, Gopalakrishna V, Vethamony P, Araligidat N, Bailey R (2002) Xbt fall rate in waters of extrem temperature: a case study in the antarctic ocean. *J Atmos Ocean Technol* 19:391–396
- Ting M, Kushnir Y, Seager R, Li C (2009) Forced and internal twentieth-century SST Trends in the North Atlantic. *J Clim* 22:1469–1481

- Trenberth K, Shea D (2006) Atlantic hurricanes and natural variability in 2005. *Geophys Res Lett* 33:L12704
- Troccoli A, Källberg P (2004) Precipitation correction in the ERA-40 reanalysis. ERA-40 Project Report Series. 13
- Uppala S et al (2005) The ERA-40 re-analysis. *Q J R Meteorol Soc* 131:2961–3012
- Vecchi G, Soden B, Wittenberg A, Held I, Leetmaa A, Harrison M (2006) Weakening of tropical pacific atmospheric circulation due to anthropogenic forcing. *Nat Biotechnol* 441:73–76. doi: [10.1038/nature04744](https://doi.org/10.1038/nature04744)
- Vidard A, Balmaseda M, Anderson D (2009) Assimilation of altimeter data in the ecmwf ocean analysis system 3. *Mon Wea Rev* 137:1393–1408
- Wijffels S, Willis J, Domingues C, Baker P, White N, Cronell A, Ridgway K, Church J (2008) Changing expendable bathythermograph fall-rates and their impact on estimates of thermosteric sea level rise. *J Clim* 21:5657–5672
- Wolff J, Maier-Reimer E, Legutke S (1997) The hamburg ocean primitive equation model. Technical report 18 German Climate Computer Center (DKRZ)